Propagation of a short proton beam through a thin plasma slab

F. Califano,[1] F. Pegoraro,[1] and S. V. Bulanov[2]
[1]*Department of Physics and INFM, Pisa University, Pisa, Italy*
[2]*General Physics Institute, RAS, Moscow, Russia*
(Received 5 May 2003; published 23 December 2003)

A one-dimensional open boundary Vlasov code is used in order to investigate the propagation of a short proton beam through a plasma slab. Collisionless regimes are assumed, where the interaction between the beam and the plasma occurs due to the self-consistent, collective, electric field. Both charge compensated (by an accompanying electron cloud) and noncompensated beams are considered.

DOI: 10.1103/PhysRevE.68.066406 PACS number(s): 52.38.Kd, 52.35.Fp, 52.35.Mw, 52.65.Ff

I. INTRODUCTION

Energetic proton beams are produced during the interaction of ultrahigh intensity, short laser pulses with plasmas. Proton acceleration is indeed one of the most important features of the petawatt pulse power regime. Laser generated proton beams are expected to have important applications ranging from proton fast ignition [1], to proton imaging [2], to localized energy deposition in biological tissues [3]. In the present experiments [4] these proton beams are emitted in short bursts of picosecond duration, are well collimated, and have a very high brilliance, but their energy spectrum is broad with maximum energies up to a few tens of MeV. High quality beams with a small energy spread are required for applications where spatially accurate energy deposition is important. A method aimed at producing such high quality beams using appropriately designed two-layer targets has been proposed in Ref. [5].

Different ion acceleration regimes are encountered in the interaction of ultraintense laser pulses with a target. When laser pulses with powers corresponding to relativistically strong fields are used, a transition is found from an essentially quasineutral lower intensity regime where the heated Boltzmann electrons accelerate the ions up to energies, per ion unit charge, of the order of the electron temperature (see, e.g., the recent calculations of the maximum ion energy presented in Ref. [6]) to a new regime where dynamical charge separation effects are dominant and a fraction of the ions can acquire an energy that is substantially larger than the electron thermal energy. Extensive investigations with multidimensional particle in cell simulations [5,7] have confirmed that collimated beams of fast protons with energies in the several MeV range can be obtained by optimizing the laser-target parameters.

Depending on the specific conditions under which the proton acceleration occurs in the laser plasma interaction, for example, whether or not the beam appears as a spatially collimated positively charged bunch in a more extended electron cloud, the proton beams may be modeled either as an initially strongly charged particle bunch or an essentially neutral (charge compensated) beam. If the beam is strongly charged, self-generated electromagnetic fields can play an important role through processes such as electrostatic Coulomb explosion and magnetic pinching. Furthermore, the beam properties change depending on whether the propagation of the beam, after it has been accelerated, occurs in an almost vacuum environment or through a dilute plasma. The process of electric charge neutralization is quite important in the context of the problem of the proton beam transport from the acceleration region to the target. For some specific applications the target may be located far from the acceleration region, in which case space charge effects can deteriorate both the beam longitudinal and the transverse emittance during its propagation (see, e,g., Ref. [8]). Evidently, such an uncontrolled change of the proton beam parameters is undesirable for most applications. Different configurations can be used in order to control the charge neutrality of the beam: the simplest is just a finite length plasma slab. After its interaction with the slab the proton beam can either gain additional electrons or lose part of the electrons that it had before interacting with the slab.

In the present paper we integrate the Vlasov-Poisson system numerically in order to study the interaction of a fast proton beam with a plasma slab and to elucidate the different processes of electric charge neutralization. These studies are also of interest for proton imaging, providing information on the reorganization of the collective electric field in the plasma exposed to the fast protons.

Different physical mechanisms are at play in the plasma beam interaction depending on the plasma density and beam energy. Here we consider relatively thin plasma conditions where collisions are unimportant in comparison with the effects of the collective electric and magnetic fields generated by the beam propagation and by its interaction with the plasma slab. As we mentioned above these thin plasma slab conditions are of interest for proton transport and proton imaging studies, but do not apply to the energy deposition phase inside a compressed pellet in the fast ignition scenario.

At the electron plasma relativistic energies and ultrafast time scales that are involved in the proton acceleration processes, both inductive electric fields, due to fast changes in the self-generated magnetic field, and electrostatic fields, due to electric charge separation, are important in determining the dynamics of the proton beam. Here we present the results of a time dependent analytical and numerical analysis where a finite length, high energy (but nonrelativistic) proton beam is followed as it propagates through a one-dimensional (1D) plasma slab. In this simplified one-dimensional analysis only electrostatic effects can be taken into account. Thus 2D and 3D effects (see, e.g., Ref. [9]), and in particular plasma lens-

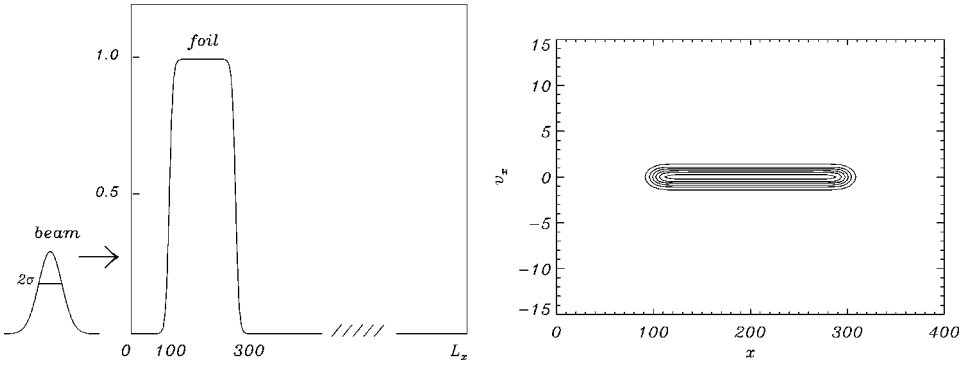

FIG. 1. Left frame: the electron and proton plasma slab (foil) at $t=0$ and the beam spatial shape. The beam is introduced in the simulation domain from the left according to the time varying boundary conditions (3). Right frame: the isocontours of the electron distribution function in a portion of the (x,v) phase space at $t=0$.

ing (see Ref. [10]), are outside scope of the adopted approximation. The numerical results presented are obtained using an ''open boundary'' Eulerian scheme for solving the one-dimensional Vlasov equation in physical and in velocity space (1D-1V) [11], which provides us with a direct representation of the evolution of the electron and proton distribution function in phase space. This open boundary scheme has been explicitly developed in order to study plasmas with a transient influx of particles and/or energy. The beam, which is initiated in vacuum and is either fully charged (no electrons) or fully compensated (as many electrons as protons), interacts with a plasma foil with density larger than that of the beam.

In the case of a charge noncompensated proton beam interacting with a plasma slab, the main physical processes at play are the sweeping of a fraction of the plasma electrons by the moving electric potential of the proton beam as it crosses the plasma slab and the oscillations at the local plasma frequency of the neutralizing electron cloud extracted from the foil as it propagates in vacuum together with the proton beam. Electron oscillations are also excited inside the plasma slab, at the plasma frequency of the electron density in the slab, in the case of very narrow (nonadiabatic) proton beams. In the case of a neutralized (charge compensated) proton beam the main physical mechanism is a beam plasma instability (see, e.g., the recent Ref. [12]) which involves the electrons of the beam and of the plasma slab. In both cases we are interested in the possible resulting spread of the proton beam in space and energy and in the spreading dependence on the beam and plasma parameters. A further point of interest is how the beam propagation can affect the plasma in the slab. This is particularly important in the case of the new diagnostics of proton imaging, since the creation by the beam of low-frequency (quasistatic) fields could in, principle, affect the proton propagation and confuse the interpretation of the field structures in the plasma. In addition, in the case of a wider plasma and for longer time scales, the proton beam plasma interaction can be of interest for the study of the wake field generation in the ion-wave regime [13].

II. OPEN BOUNDARY VLASOV CODE

We employ a numerical code that integrates the Vlasov-Poisson system of equations for a two-component plasma in the 1D-1V phase space in the nonrelativistic limit:

$$\frac{\partial f_a(x,v,t)}{\partial t}+v\frac{\partial f_a(x,v,t)}{\partial x}-\mu_a\frac{\partial \phi}{\partial x}\frac{\partial f_a(x,v,t)}{\partial v}=0,$$

$$a=e,i, \tag{1}$$

$$\frac{\partial^2\phi}{\partial x^2}=\int f_e(x,v,t)dv-\int f_p(x,v,t)dv, \quad E=-\frac{\partial\phi}{\partial x}, \tag{2}$$

where quantities are normalized with a characteristic density $\overline{n}$, the electron mass m_e, the Debye length λ_{De}, the inverse of the plasma frequency ω_{pe}^{-1}, and a characteristic electric field $\overline{E}=m_e\omega_{pe}v_{the}/e$. Here v_{the} is the electron thermal speed and $\mu_a=m_e/m_a$.

The initial and the boundary conditions and the initial form of the electron distribution function are sketched in Fig. 1. The simulation box extends spatially from $x=0$ to $x=L_x$ (in λ_{De} units). The initial conditions correspond to a neutral electron-ion plasma slab situated close to the left boundary. The density of the slab is constant (and equal to 1) on a plateau $270\lambda_{De}$ long with two ramps of $40\lambda_{De}$. The temperatures of the electrons and protons in the plasma slab are equal ($T_e=T_i$). From the left boundary ($x=0$) we inject a proton beam (together with an equally shaped electron beam in the charge neutralized case) by varying the boundary conditions of the electron and proton distribution functions in time. This corresponds to the following boundary conditions (at a fixed time instant):

$$f_a^{>}(v)=\text{given for} \quad v\geqslant 0, \quad \phi=0 \quad \text{at } x=0, \tag{3}$$

$$f_a^{<}(v)=\text{given for} \quad v\leqslant 0, \quad \frac{\partial\phi}{\partial x}=0 \quad \text{at } x=L_x. \tag{4}$$

The last condition corresponds to $E=0$ at $x=L_x$ and is valid until fast particles reach the right boundary. At that moment the simulation is stopped. In the case of the charge noncompensated beam, this condition implies that no electric field is generated by the proton beam in front of itself, as consistent with the causality requirement. In this model the noncompensated beam is considered to originate from a neutral source outside the simulation box ($x<0$) which is left negatively charged as the beam propagates. This negative charge outside the simulation box ensures that, in the 1D configura-

tion considered here, the electric field due to the beam vanishes in front of the beam. In order to focus our attention on the interaction of the charged beam with the plasma slab in the simulation, we keep this source term constant in time and disregard the effect of the electric field of the beam on it. On the other hand, this electric field causes the protons at the back of the pulse to experience, before interacting with the plasma slab, a retarding electric field which is twice as large as that which would be produced by the Coulomb explosion while the protons at the front experience no electric field. We must thus ensure that, in the case of a noncompensated beam, its travel time before it reaches the plasma slab be short compared to its Coulomb explosion time. In practice, in the case of noncompensated beams, this Coulomb explosion is responsible for a considerable velocity spreading of the beam in its initial propagation phase even before it reaches the plasma slab and becomes neutralized. This initial velocity spreading is then transformed into a spatial spreading as the beam propagates to the right of the plasma slab by the ballistic evolution of the distribution function.

In our numerical runs the proton beam has a Gaussian shape with half-width $\sigma_{\rm beam}$ (see Fig. 1, first frame) ranging between $35\lambda_{De}$ and $3.5\lambda_{De}$, mean velocity $u_0=5v_{the}$, and maximum density n_b ranging from 0.05 to 0.75 corresponding to a ratio Δq between the total number of protons in the beam and in the plasma slab ranging from $\approx 1.5\%$ to $\approx 15\%$. The beam temperature was taken equal to the plasma slab temperature. We take the mass ratio $\mu_p=1/1836$. The numerical algorithm adopted in these simulations, including the boundary conditions strategy, is described in Ref. [11]. The specific value of the adopted beam velocity, $u_0=5v_{the}$, was chosen as the best compromise between the requirement that the proton beam moves much faster than the thermal electrons and the numerical constraints of a Vlasov code where the velocity space interval $-v_{max}<v<v_{max}$ must contain the beam velocity $v_{max}\gg u_0$, and the corresponding mesh size $dv=v_{max}/N_v$ must be smaller than the proton thermal velocity, $dv\ll v_{th,p}$.

The initial plasma slab configuration is not a Vlasov equilibrium and the electrons expand into the vacuum region creating a charge separation at the plasma vacuum interface which slows down the electron expansion and leads to an ambipolar expansion of the plasma. Due to the large beam velocity adopted in this model, this plasma slab expansion is slow compared to the beam propagation and does not affect our numerical results significantly. The same considerations apply to the thermal spreading of the compensated ''long'' beam ($\sigma_{\rm beam}=35$). Control numerical simulations of the beam propagation without the plasma slab (briefly reported and discussed in the Appendix) confirm that the thermal spreading of long beams is negligible. On the other hand, in the case of a ''short'' beam ($\sigma_{\rm beam}=5.3$), the spreading, defined by the change with time of the value of the beam width σ, becomes significant and, over a distance of $1000\lambda_{De}$ corresponding to the normalized time $t\approx 200$, can be estimated to be of the order of 40%.

As a final test, we have also verified that the results presented for both long and short beams remain valid in the case of a wider plasma slab (we have performed simulations up to a slab width of $500\lambda_{De}$).

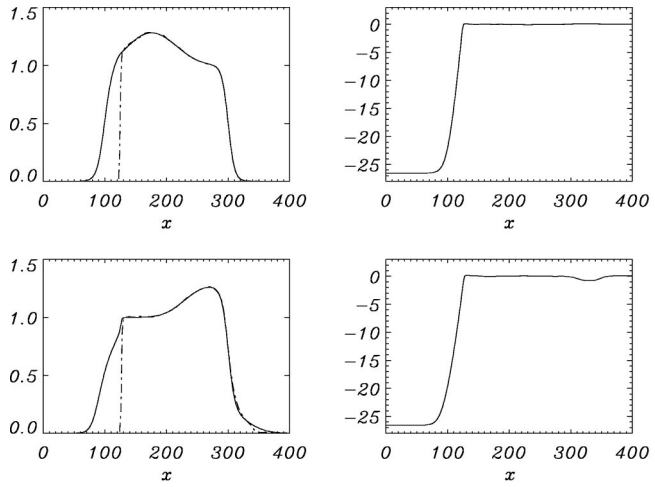

FIG. 2. Left frames: the proton and electron densities (continuous and dash-dotted lines, respectively) at $t=60$ (upper frame) and at $t=80$ (lower frame). Right frames: the electric field at the same time instants.

III. CHARGE NONCOMPENSATED BEAMS

In the limit where the ramp-up time $\tau_{\rm rump}\approx\sigma_{\rm beam}/u_0$ of the electric field carried by the beam is longer than ω_{pe}^{-1}, the electrons in the slab redistribute their density almost adiabatically following the beam propagation, as shown in Fig. 2 for an initially noncompensated proton beam with maximum density $n_b=0.3$, $\Delta q\simeq 10\%$, and dimensionless half-width $\sigma_{\rm beam}=35$ (in this simulation $L_x=3000$). Here the electron and proton densities and the electric field are shown vs x at $t=60$ when the proton beam has just entered the slab and at $t=80$ just before it comes out from the slab. In Fig. 3 we show (upper frames) the electron and proton (thick line) densities vs time inside the plasma slab and in the right (decreasing) density ramp where, at $t=0$, $\langle n_e\rangle=\langle n_p\rangle=0.5$. We see that small amplitude plasma oscillations are excited by the beam with $\delta n_e\sim 2\%$ and $\delta n_e\sim 10\%$ (with respect to the local mean value) inside the plasma and in the ramp, respec-

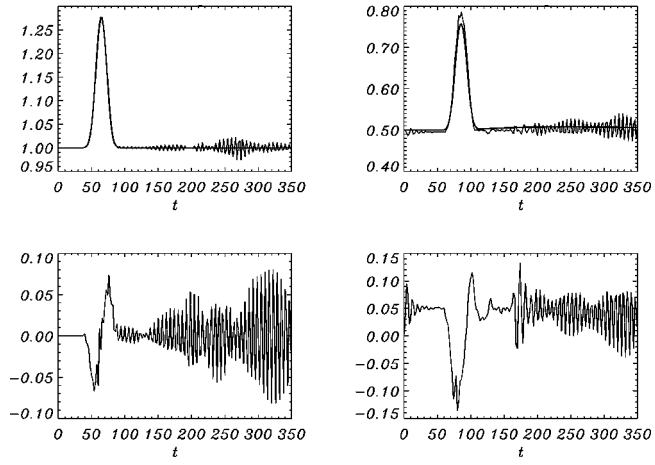

FIG. 3. Upper frames: the electron and proton densities (thick line) vs time at $x=200$ and $x=300$. Lower frames: the same for the electric field.

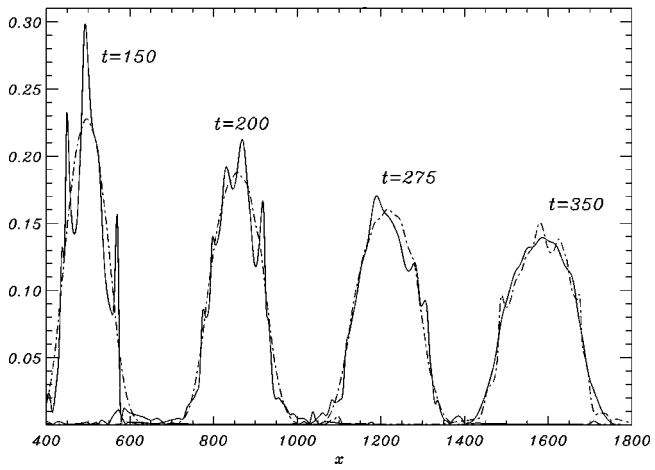

FIG. 4. The electron and proton densities (continuous and dash-dotted lines, respectively) after crossing the plasma slab at $t=150$, 200, 275, and 350.

tively. The corresponding electric field is shown in the lower frames.

After crossing the plasma slab, the plasma beam propagates in the vacuum region at nearly the initial mean velocity u_0 together with the neutralizing electrons, as shown in Fig. 4, which is a composite of images of the electron and proton densities at $t=150$, 200, 275, and 350. The total number of protons in the beam is practically equal to that of the initial beam (before entering the slab). The electrons traveling with the beam fully neutralize the total initial charge of the beam. This global neutralization is a consequence of the fact that in a one-dimensional configuration the ions must rip off an equal number of electrons from the slab since any net charge imbalance would produce an electrostatic energy associated with the proton beam that increases proportionally with the distance between the plasma slab and beam position. On the contrary, if the proton beam is globally neutral, the electric energy of the system remains finite as the beam propagates away from the slab.

In this 1D simulation the resulting unbalanced positive charge in the slab is later compensated by a slow flow of protons through the left ramp of the slab (not shown in Fig. 4) towards the left boundary of the simulation box. This return proton flow restores the global neutrality of the plasma slab on a time scale of the order of the inverse ion plasma frequency, calculated with the density of the noncompensated protons in the slab. We observe however that in higher dimensional configurations this process will compete with the transverse motion of the electrons in the plasma slab that will contribute to neutralize the region left charged by the interaction with the beam.

The interaction between the proton beam and the slab produces no significant heating of the slab electrons. In the absence of collisions, the protons in the beam could transfer part of their energy to the plasma slab electrons by exciting a Buneman-type instability [14]. However, for the parameters of the simulation in Fig. 2, this mechanism is not effective since the instability growth rate γ_{Bun}, calculated near threshold for a homogeneous plasma and normalized with the slab plasma frequency, scales as $(n_b m_e/m_p)^{1/3}$, where n_b is the normalized proton beam density. Such a growth rate leads to an *e*-folding time greater than the beam crossing time, $\gamma_{\mathrm{Bun}}\tau_{\mathrm{trans}}<1$, and to an e-folding distance considerably longer than the beam length, $\sigma_{\mathrm{beam}}<u_0/\gamma_{\mathrm{Bun}}$.

The electron density in the beam is modulated by Langmuir oscillations (at the local beam plasma frequency) that are excited in the ramp-down region of the plasma slab. These electron oscillations decay as the beam propagates due to phase space mixing (caused by the inhomogeneity of the beam density), without causing any significant modulation of the proton beam, but heating the distribution of the traveling electrons as shown in Fig. 5 where we draw the electron distribution function isocontours at the same time instants as in Fig. 4. From Fig. 4 we observe that, as the beam propagates, its width increases and, correspondingly, its maximum density decreases at a rate faster than the rate predicted by the thermal expansion of a neutralized proton beam at the initial beam temperature. This enhanced ''thermal'' beam spreading is a kinetic consequence of the initial stretching in velocity space of the noncompensated beam before it enters the slab and is caused by the differential deceleration (see the Appendix) produced by the self-generated electric field (i.e., by the Coulomb explosion) before the beam becomes neutralized. This ballistic evolution of the proton beam distribution function is shown in Fig. 6 where the evolution of the proton distribution function in the case of a noncompensated (upper frame) beam is compared to that, discussed in the following section, of a compensated (lower frame) beam.

From a detailed analysis of the electron distribution function at different time instants, we observe that some fast particles are generated close to the right edge of the plasma slab and propagate with typical velocities up to two-three times the beam mean velocity (see Fig. 3, right frames). This effect can be easily modeled by referring to the limit of a very short and fast proton beam interacting with a very thin plasma slab. The electrons extracted from the plasma behind the proton beam feel a negative electric field E that depends on their initial coordinate. This electric field accelerates the electrons until they overtake the proton beam which propagates with velocity u_0. The velocity and position of these electrons are given in dimensional units by $v(t)=eEt/m_e$ and $x(t)=eEt^2/2m_e$. The acceleration time is equal to the time $2m_e u_0/eE$ it takes the electrons to overtake the proton beam. When the electrons overtake the beam their velocity is equal to $2u_0$, i.e., twice as large as the proton velocity. In addition, the electrons gain energy during the breaking of the plasma oscillations where they are accelerated by the electric field of the waves with the phase velocity towards the lower plasma density [15,16] region in the slab ramp. In the case of a long proton beam the amplitude of these oscillations is small and only few fast electrons are produced. The most energetic electrons overtake the proton beam, but the electric field that they generate is not sufficiently strong to affect its propagation significantly. Nevertheless, the simulation is interrupted when these fast electrons reach the right boundary as they introduce a small but detectable perturbation in the boundary conditions.

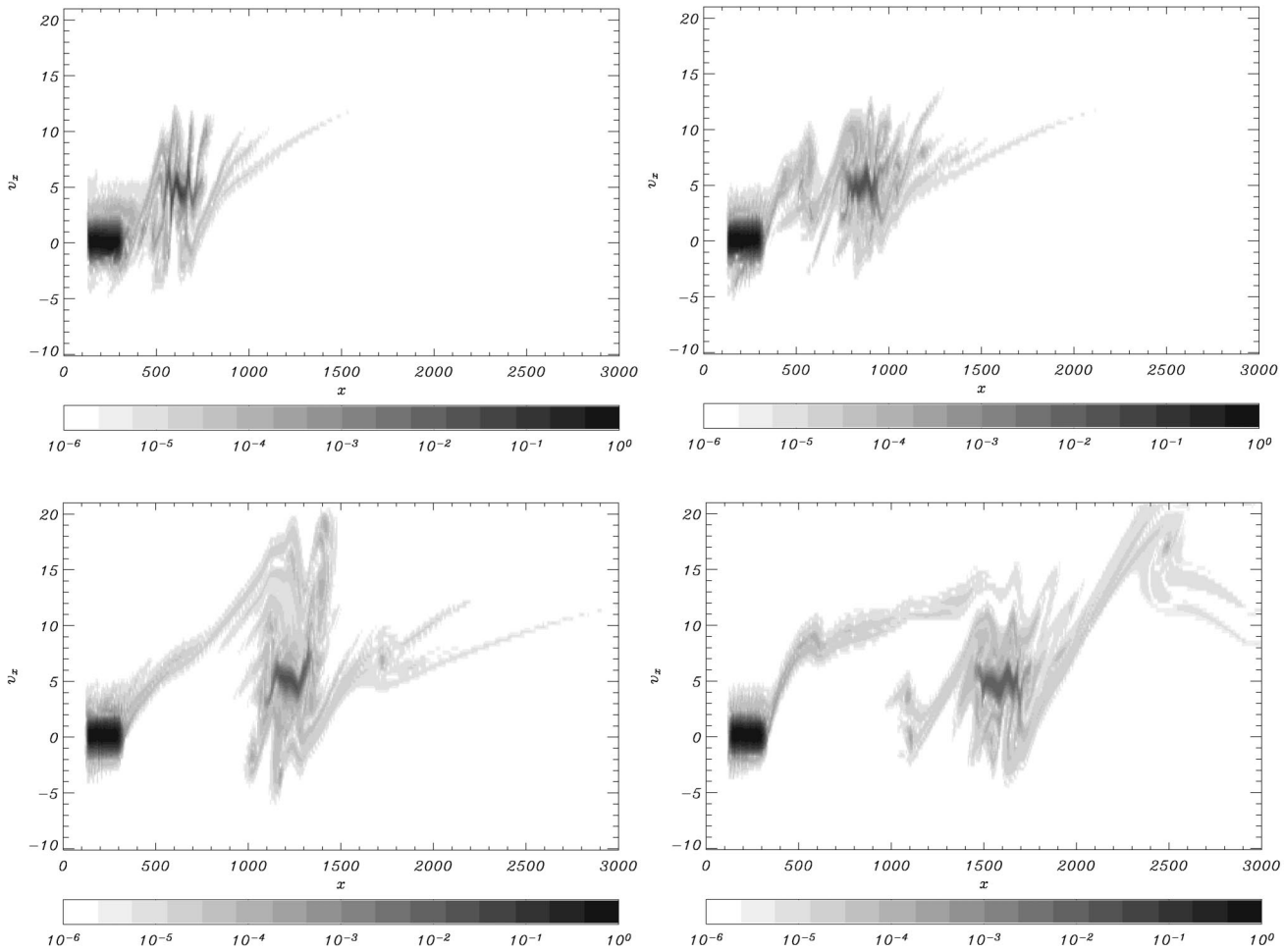

FIG. 5. The electron distribution function at the same time instants as in Fig. 4.

We consider now the case of a very short proton beam with $\sigma_{\text{beam}}=5.3$, $n_b=0.75$, $\Delta q\simeq 5\%$, and $L_x=2500$. In this case, the adiabatic approximation does not apply and strong Langmuir oscillations are excited in the plasma slab in the wake of the proton beam, as shown in Fig. 7 where the electron and proton densities and the electric field are plotted vs x at $t=60$, when the proton beam has just entered the slab, and at $t=80$, just before it exits the slab. These strong Langmuir oscillations, with amplitudes ranging, with respect to their initial values, from $\delta n_e\simeq 20\%$ inside the slab to $\delta n_e\simeq 40\%$ inside the ramp, lead to a strong and rapid heating of the electrons in the plasma slab, as shown by the electron distribution function in phase-space in Fig. 8, first frame, at $t=100$. Subsequently, due to propagation and phase mixing effects, the amplitude of these plasma oscillations decreases. Small proton depletions with $\delta n_p\sim 3$–$4\,\%$ are produced starting from $t\sim 100$ and persist till the end of the simulation. The cavity formation process will be discussed in more detail in the following section. The breaking of the large amplitude plasma waves, excited at the right slab edge region $x\sim 300$ when the beam exits from the plasma slab, produces a population of ''free'' electrons some of which propagate in front of and some behind the proton beam, as shown in Fig. 8. The density of these free electrons is sufficient to generate an electric field E that accelerates the front of the beam and slows down its back. In turns, this field accelerates the electron at the back, as discussed qualitatively above, and slows down the electrons at the front of the beam making them oscillate around the proton beam with characteristic time $2m_e u_0/eE$. The resulting spread of the proton beam, as it propagates outside the plasma slab, is illustrated in Fig. 9 where we plot the proton and electron density at different time instants. This spatial spread is due to the combined effects of the enhanced ballistic expansion caused by the initial phase of Coulomb explosion discussed in the preceding section and of the distortion caused by the field of the free electrons. As indicated by the evolution of the proton distribution function in velocity space, Fig. 10, the velocity spread caused by the initial Coulomb explosion is small compared to that due to the electric field of the free electrons, which stretches the proton distribution function towards both slower velocities (at the back) and larger velocities (at the front).

IV. COMPENSATED BEAMS

In the case of a long, charge compensated beam, with the same parameters of the noncompensated long beam dis-

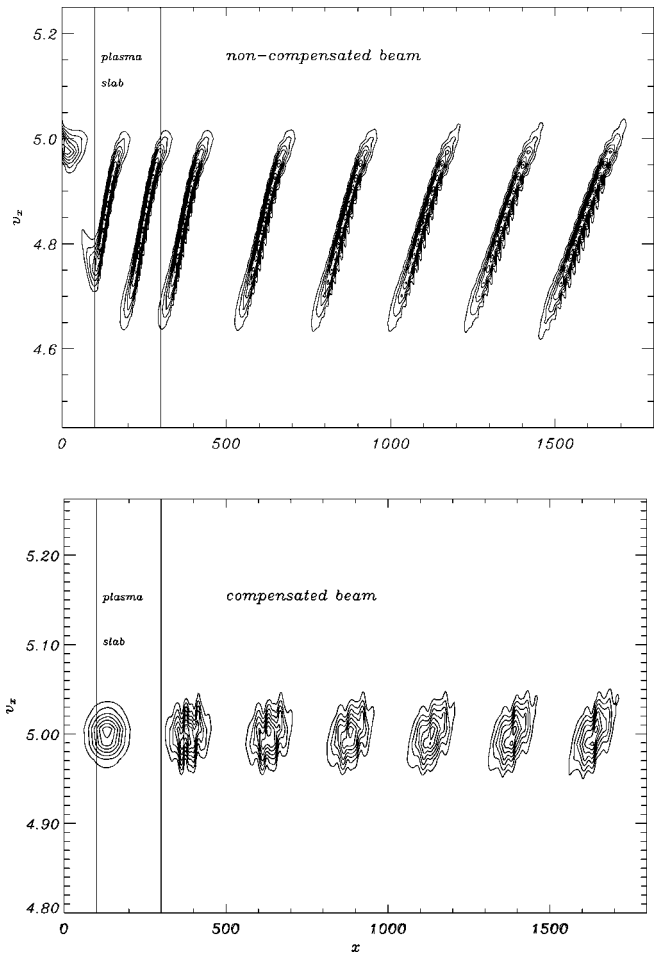

FIG. 6. Upper frame: the long noncompensated beam proton distribution function at $t=25$, 50, 75, 100, 150, 200, 250, 300, and 350. Lower frame: the same for a long compensated beam at $t=50$, 100, 150, 200, 250, 300, and 350.

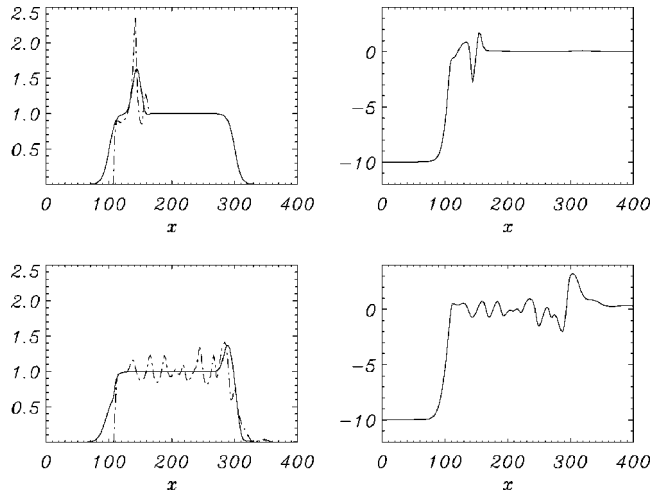

FIG. 7. Left frames: the proton and electron densities (continuous and dash-dotted lines, respectively) at $t=32$ (upper frame) and at $t=62$ (lower frame). Right frames: the electric field at the same time instants.

cussed previously, the velocity difference between the beam electrons and the plasma electrons inside the plasma slab excites a fast growing two-electron beam instability (see, e.g., the pioneering simulations in Ref. [17] and, in the recent literature, [12,18]), with a growth rate γ_{el} that scales at threshold as $n_b^{1/3}$. This instability causes strong Langmuir small scale oscillations (at the slab plasma frequency), as shown in Fig. 11 inside the plasma slab at $t=70$ before the beam exits the slab. These electron density oscillations slowly damp as the beam propagates out of the plasma slab. The proton beam emerges from the slab and propagates in vacuum with nearly the initial velocity, $u_0=5$, together with the neutralizing electrons. In the charge compensated case we can expect that the energy transfer between the protons in the beam and the electrons inside the slab is even weaker than in the noncompensated case because the electrons that accompany the proton beam will shield the proton field. If we consider a Buneman-type instability involving the slab and the beam protons, we find that in the limit case where, as a result of the two-electron beam instability, a single hot electron population is formed inside the plasma slab the growth rate of the proton instability scales as the frequency of an ion sound wave times $n_b^{1/3}$ [19]. The proton beam spatial spread, when it exits the plasma slab, is negligible due to the absence of the velocity spread caused, in the case of the noncompensated beam, by the Coulomb explosion before the beam enters the slab. Similar to the noncompensated case, the electron density in the beam propagating in vacuum to the right of the plasma slab exhibits fluctuations at the beam plasma frequency. The beam propagation in the vacuum region is shown in Fig. 12, which is a composite of images of the electron and proton densities at $t=125$, 175, 225, and 275. We see that, as soon as the proton beam exits from the slab, the Gaussian-like spatial shape of the beam is significantly modified (contrary to the noncompensated case, see Fig. 4 dash-dotted lines), showing the presence of small scales modulations. These proton beam modulations are first generated by the plasma waves produced by the beam plasma instability in the slab (these waves are absent in the noncompensated case) and then grow during the beam propagation in vacuum on a time scale much slower than the beam plasma frequency. The mechanism which produces these local inhomogeneities is similar to the cavity formation process by ponderomotive effects and will be discussed below in the case of the plasma oscillations in the slab. The effect of the Langmuir oscillations in the plasma slab and in the propagating beam on the electron distribution function is shown in Fig. 13 at the same time instants as in Fig. 12. Similar to the noncompensated case, the plasma oscillations in the slab ramp cause the formation of a population of free electrons that propagate both in front of and behind the proton beam, as shown in Fig. 14 where we plot the electric field at $t=100$, after the beam exits from the slab, and at $t=250$. In this figure we observe that the electric field is not zero at the left boundary at $t=250$, even if the beam is compensated, due to the emission of electrons by the left ramp slab, which are allowed to exit freely from the left boundary, as consistent with the boundary conditions given by Eqs. (3).

Increasing or decreasing the number of particles in the

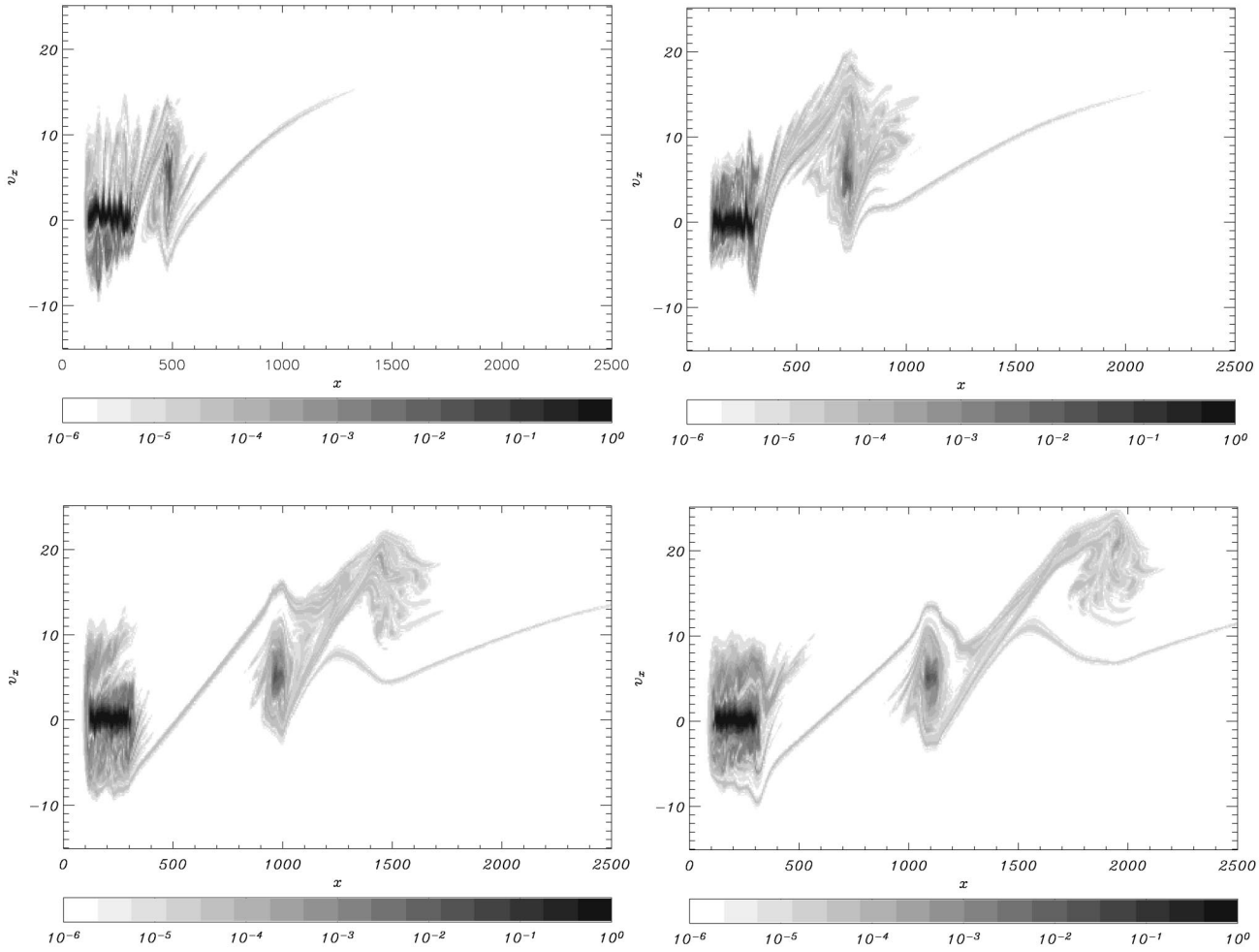

FIG. 8. The electron distribution function at $t=100$, 150, 200, and 225.

long compensated beam does not change the above picture qualitatively. At rather small beam densities the amplitude of the oscillating electric fields is essentially in agreement with the quasilinear estimate for a homogeneous plasma (see, e.g., Ref. [20], Sec. 10.5, Eq. (10.5.9)), once the ratio between the width of the plasma slab and the width of the beam is included. At higher beam densities, such as those shown in Fig. 11, the amplitude of the oscillating fields is found to be

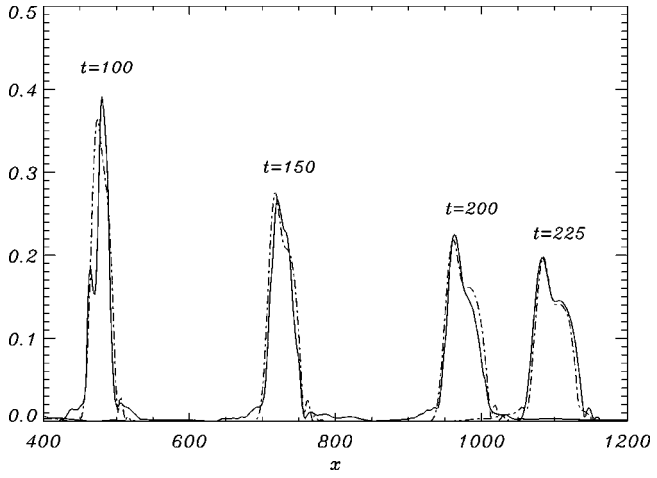

FIG. 9. The electron and proton densities (continuous and dash-dotted lines, respectively) after the plasma slab at $t=100$, 150, 200, and 225.

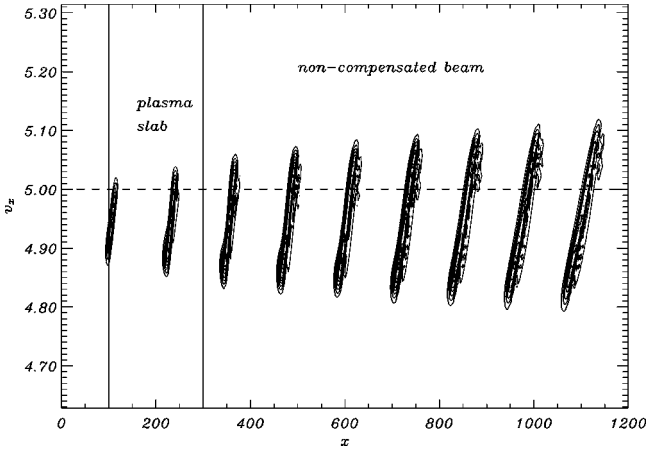

FIG. 10. The beam proton distribution function from $t=25$ to $t=225$ with every $\Delta t=25$.

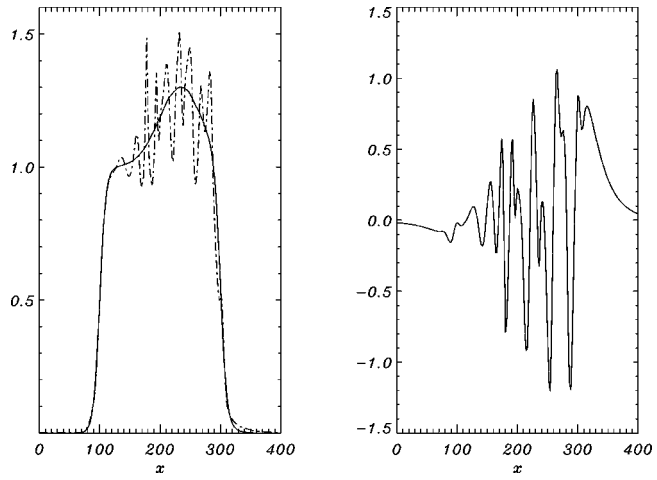

FIG. 11. Left frame: the proton and electron densities (continuous and dash-dotted lines, respectively) at $t=70$. Right frame: the electric field at the same time instant.

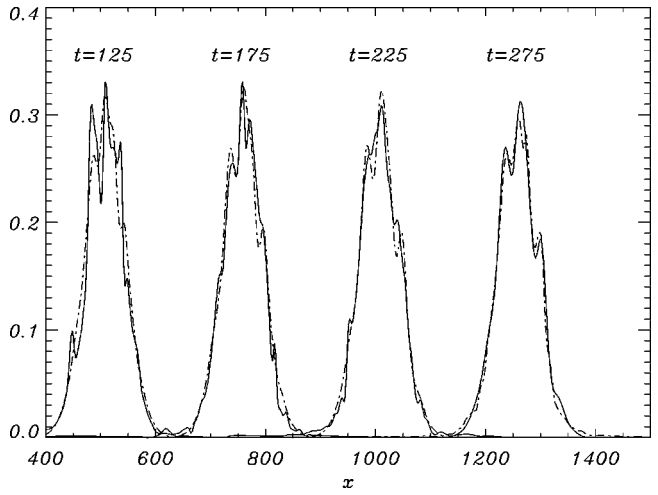

FIG. 12. The electron and proton densities (continuous and dash-dotted lines, respectively) after existing the plasma slab at $t=125$, 175, 225, and 275.

smaller than the quasilinear estimate and to grow with the beam density slower than $n_b^{1/2}$.

In the case of a short charge compensated beam, with the same parameters of the noncompensated short beam discussed in the preceding section, we see that the difference between charge compensated and noncompensated beam is less marked than in the case of longer (adiabatic) beams. A short compensated beam produces a strong oscillating elec-

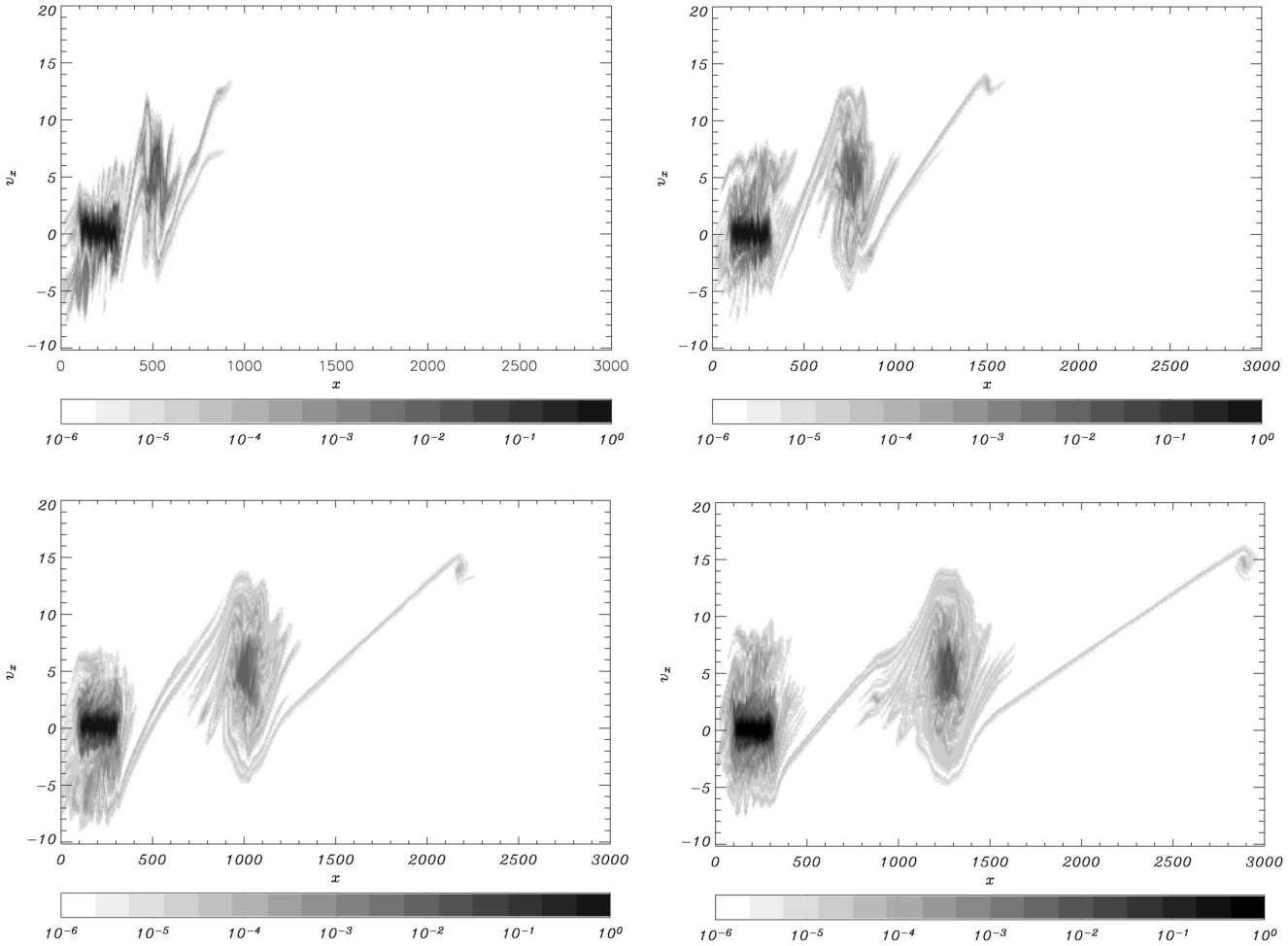

FIG. 13. The electron distribution function at the same time instants as in Fig. 12.

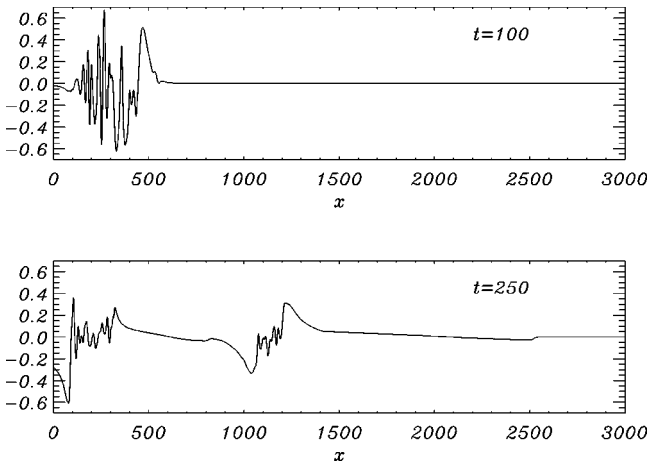

FIG. 14. The electric field vs x at $t=100,\ 250$.

tric field wake in the plasma slab, as shown in Fig. 15 where we plot the proton and electron densities (left frames) and the electric field (right frames) at $t=32$ and $t=55$. This interaction is strong enough to perturb the charge neutrality of the beam.

Similar to the short noncompensated case, this causes a considerable velocity spread as the beam propagates to the right of the plasma slab, as shown by the proton distribution function evolution in Fig. 16 and by the electron and proton beam density evolution in Fig. 17 after the beam exits the slab. This velocity spread is a consequence of the electric field arising from the partial charge separation between the protons in the beam and the electrons (involved in the beam plasma instability in the slab) that propagate with it, and by the free electrons generated by the slab inhomogeneity. The electric field is shown in Fig. 18 at $t=100$ and $t=250$.

As in the case of a long compensated pulse, if the particle's density in the short proton beams is increased, the amplitude of the Langmuir oscillations inside the plasma slab becomes larger and the proton density in the slab starts to be significantly perturbed and forms slowly deepening cavities.

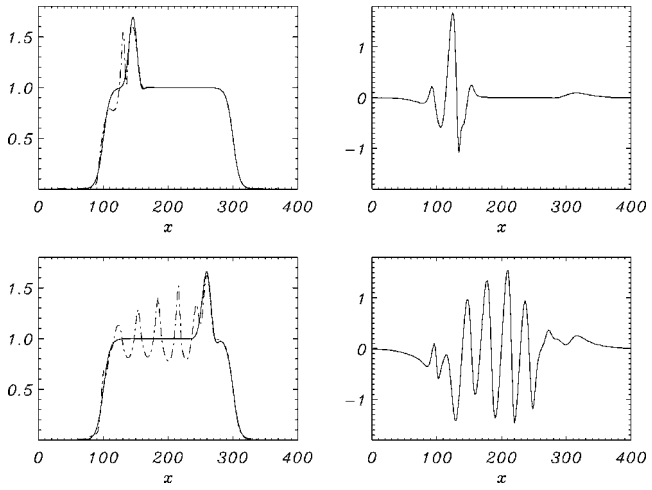

FIG. 15. Left frames: the proton and electron densities (continuous and dash-dotted lines, respectively) at $t=32$ (upper frame) and at $t=55$ (lower frame). Right frames: the electric field at the same time instants.

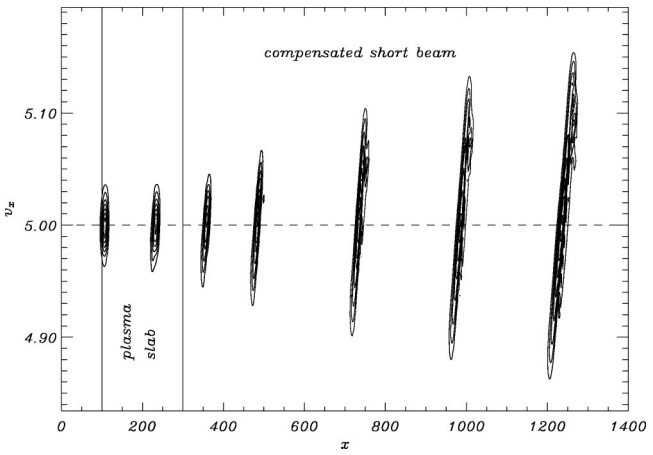

FIG. 16. The beam proton distribution function at $t=25,\ 50,\ 75,\ 100,\ 150,\ 200,$ and 250.

These cavities appear quite markedly in Fig. 19 for a short beam with density $n_b=0.75$, $\sigma=5.3$ and a plasma slab $370\lambda_{De}$ long. We see the deepening of cavities in the proton density spatially modulated with a scale length of half the wavelength of the electron Langmuir oscillations, consistent with a nonlinear ponderomotive drive of the cavities by the (standing) electron oscillations [21] in the plasma slab.

V. CONCLUSIONS

The simulations that we have performed of the interaction of a proton beam with a thin plasma slab show the formation of oscillating electric fields in the plasma slab excited by the beam propagation, both in the case of charge compensated and noncompensated beams. In the case of long beams (adiabatic interaction), these fields are much stronger in the charge compensated case. In the case of a short beam (nonadiabatic interaction) the difference between noncompensated and compensated beams is less marked.

These electric fields can cause spatial and velocity spreading of the proton beam. This spreading is significant in those

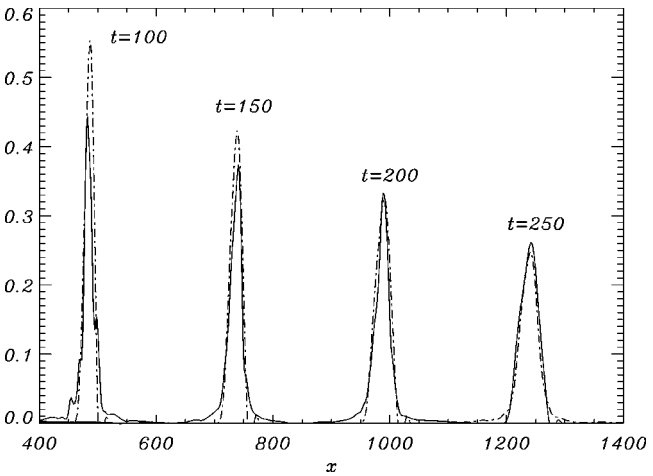

FIG. 17. The electron and proton densities (continuous and dash-dotted lines, respectively) after existing the plasma slab at $t=100,\ 150,\ 200,$ and 250.

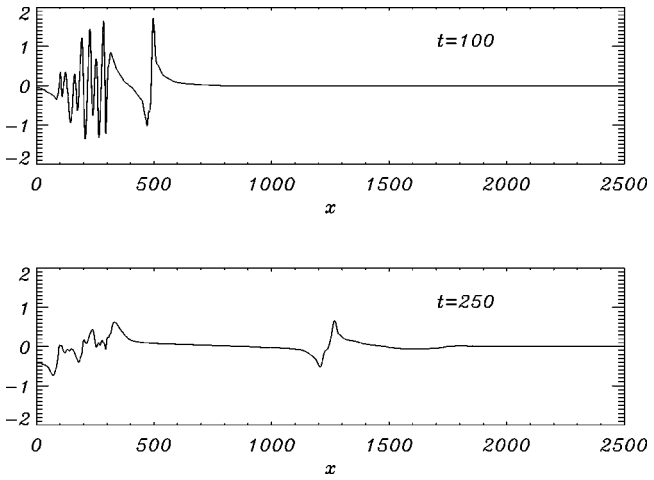

FIG. 18. The electric field vs x at $t=100$, 250.

cases where the interaction between the beam and the plasma slab produces a population of free fast electrons or leaves the beam propagating outside the slab not fully quasineutral, even if the total charge of the propagating beam is well compensated. This happens, e.g., in the case of short beams, independent of whether, before interacting with the plasma slab, the beams were charge compensated or noncompensated. The beam propagation to the right of the plasma slab corresponds to that of a globally neutralized beam. However, in particular, in the case of short beams, a completely ambipolar configuration is not reached until the Langmuir oscillations of the neutralizing electron cloud are quenched by phase mixing and the free electrons propagating in front and at the back of the beam are reabsorbed into the beam due to the electric forces acting on them.

In all the cases examined, the total energy of the proton beam is essentially unchanged by its interaction with the plasma slab. In the case of a charge compensated beam the total energy in the oscillating electric fields inside the slab is a fraction of the total ordered kinetic energy of the electrons that propagate with the beam.

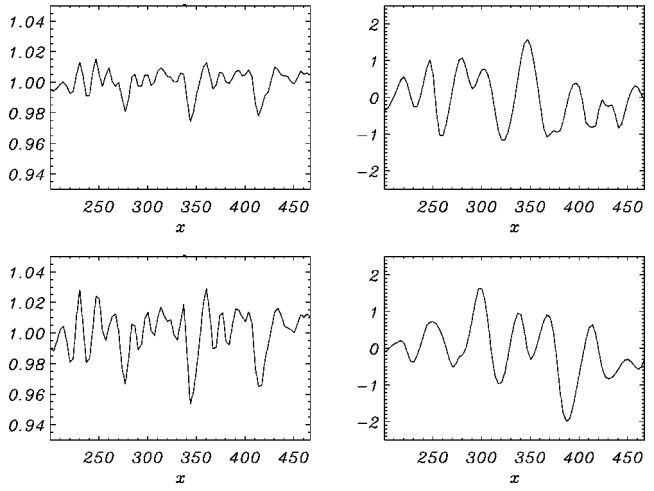

FIG. 19. The proton density and the electric field at $t=150$, 200 for the short, compensated beam case with a longer slab of length $370\lambda_{De}$.

In a one-dimensional configuration such as the one considered in this paper, the electric field can only accelerate or decelerate the protons, whereas the technique of proton imaging relies on the proton deflection by a (slowly varying) field component orthogonal to the direction of the proton propagation. Thus the simulations that we have presented cannot be used directly to establish the limits of applicability of the test particle approximation used to calculate the proton deflection in the proton imaging technique and, in particular, to determine whether the electric fields generated by the proton beam could mask the effects of the ''true'' electromagnetic fields inside the plasma. In addition, the ratio between the density of the proton beam and that of the plasma slab is much larger in our simulations than that used in the proton imaging technique. However if we introduce an efficiency factor η which represents the fraction of the ordered kinetic energy of the electrons that accompany the beam that is transformed into energy of the fluctuating electromagnetic energy, we can expect that the beam generated fields could lead to a ''background noise'' in the deflection patterns measured by the proton imaging technique with a jitter deflection angle of the order of $(2L\sigma\eta/d_b^2)^{1/2}(cm_e/m_iu_0)$, where L is the slab width and d_b the electron skin depth evaluated with the beam density.

ACKNOWLEDGMENTS

We are glad to acknowledge A. Mangeney for interesting discussions. Part of this work was performed in the frame of the INTAS Project No. 01-0233. Part of this work was supported by the INFM Parallel Computing Initiative.

APPENDIX: BEAM THERMAL EXPANSION

In order to separate the effects of the beam interaction with the plasma slab from those arising from the unperturbed beam propagation in vacuum, we have performed control numerical simulations with beam parameters equal to those used in the runs reported above and no plasma slab, and we have compared the results obtained in this way to those with plasma slab and to simple analytical estimates.

We consider a charge compensated Gaussian beam with an initial proton distribution function given in a comoving reference frame at $t=0$ by

$$f_p(x_0,v_0)=\frac{n_0}{(\pi\mu_p)^{1/2}}\exp[-x_0^2/(2\sigma^2)-v_0^2/\mu_p], \quad \text{(A1)}$$

and a corresponding electron distribution with the same temperature. The distribution function of Eq. (A1) does not correspond to a Vlasov equilibrium and evolves in time. If we assume exact quasineutrality, no electric field is present and the proton distribution function at time t is obtained from Eq. (A1) using the characteristics

$$x(t)=x_0+v_0t, \qquad v(t)=v_0, \qquad \text{(A2)}$$

and reads

$$f_p(x,v,t)=\frac{n_0}{(\pi\mu_p)^{1/2}}\exp[-(x-vt)^2/(2\sigma^2)-v^2/\mu_p]. \tag{A3}$$

However, in the very first phase of the beam expansion, when the electrons move outwards faster than the ions before the beam expansion becomes ambipolar, an electric field is generated, which produces an initial velocity spread that is transformed into a spatial spread as the beam propagates. If we take this velocity spread of the form $\delta v_0=V'x_0$, we obtain

$$f_p(x_0,v_0,t_0)=\frac{n_0}{(\pi\mu_p)^{1/2}}\times\exp[-x_0^2/(2\sigma^2)-(v_0-V'x_0)^2/\mu_p] \tag{A4}$$

which gives

$$f_p(x,v,t)=\frac{n_0}{(\pi\mu_p)^{1/2}}\exp[-(x-vt)^2/(2\sigma^2)-[v-V'(x-vt)]^2/\mu_p] \tag{A5}$$

instead of Eq. (A3). Then, the time dependence of the density at the center of the beam ($x=0$ in the comoving frame) due to its thermal expansion is given by

$$n(t)/n(0)=[(1+tV')^2+t^2\mu_p/(2\sigma^2)]^{-1/2}, \tag{A6}$$

which predicts an initial density decrease linear in t for $V'\neq 0$.

In Fig. 20 we plot the time evolution of the maximum beam density $n(t)$ in the case of a short, compensated beam which propagates in the absence of the plasma slab (curve A), and in the presence of the plasma slab (curve C). The beam parameters are those of the short, compensated beam discussed in the second part of Sec. IV (see Figs. 15–17). Curve B in Fig. 20 represents the analytical expression, Eq. (A6), with $V'\approx 0.001$. We see that curve A and curve B are practically superposed, and show that the expansion of the compensated beam in vacuum is simply the ballistic evolution of the initial distribution function. On the other hand, curve C shows that as soon as the beam enters the plasma slab, $t\approx 15$, electric field effects play a major role and produce a space dependent velocity spread. This additional velocity spread can be represented as a redefinition of V' in Eq. (A6) and is responsible of the faster decreasing slope of curve C with respect to curves A and B for $t<100$. In addition, after the beam exits the plasma slab, the self-consistent electric fields of the accelerated particles and/or the lack of exact (local) quasineutrality increase the beam spreading further with respect to the case where the beam propagates in vacuum without interacting with the plasma slab.

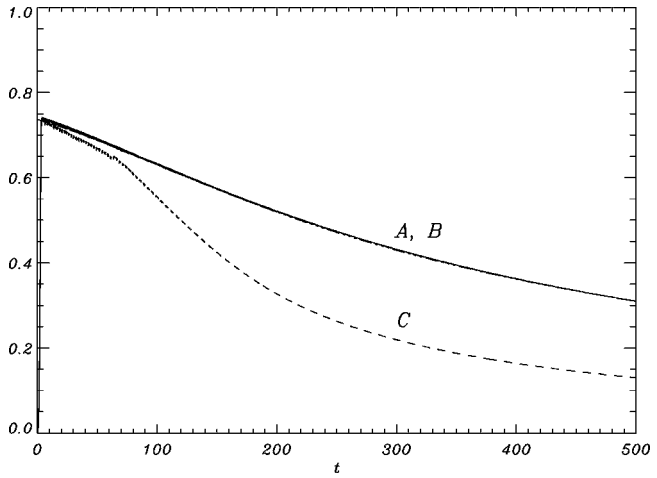

FIG. 20. The time evolution of the maximum beam density $n(t)$ for a short, compensated beam without the plasma slab (curve A), in the presence of the plasma slab (curve C). Curve B represents the analytical expression, Eq. (A6), with $V'\approx 0.001$.

[1] M. Roth *et al.*, Phys. Rev. Lett. **86**, 436 (2001); V.Yu. Bychenkov *et al.*, Plasma Phys. Rep. **27**, 1017 (2001).

[2] M. Borghesi *et al.*, Plasma Phys. Controlled Fusion **43**, A267 (2001); M. Borghesi *et al.*, Phys. Rev. Lett. **88**, 135002 (2002); M. Borghesi *et al.*, Phys. Plasmas **9**, 2214 (2002); M. Borghesi *et al.*, Rev. Sci. Instrum. **74**, 1688 (2003).

[3] S.V. Bulanov and V.S. Khoroshkov, Plasma Phys. Rep. **28**, 453 (2002); S.V. Bulanov *et al.*, Phys. Lett. A **299**, 240 (2002).

[4] A. Maksimchuk *et al.*, Phys. Rev. Lett. **84**, 4108 (2000); E. Clark *et al.*, *ibid.* **85**, 1654 (2000); S. Hatchett *et al.*, Phys. Plasmas **7**, 2076 (2000); R. Snavely *et al.*, Phys. Rev. Lett. **85**, 2945 (2000); A. Mackinnon *et al.*, *ibid.* **86**, 1769 (2001); A. Mackinnon *et al.*, *ibid.* **88**, 215006 (2002); M. Hegelich *et al.*, *ibid.* **89**, 085002 (2002).

[5] T. Esirkepov *et al.*, Phys. Rev. Lett. **89**, 175003 (2002); S.V. Bulanov *et al.*, Plasma Phys. Rep. **28**, 453 (2002).

[6] P. Mora, Phys. Rev. Lett. **90**, 185002 (2003)

[7] T. Esirkepov *et al.*, Pis'ma Zh. Eksp. Teor. Fiz. **70**, 80 (1999) [JETP Lett. **70**, 82 (1999)]; S. Bulanov *et al.*, *ibid.* **71**, 407 (2000); Y. Sentoku *et al.*, Phys. Rev. E **62**, 7271 (2000); F. Pegoraro *et al.*, IEEE Trans. Plasma Sci. **28**, 1226 (2000); H. Ruhl *et al.*, Fiz. Plazmy **27**, 387 (2001) [Plasma Phys. Rep. **27**, 363 (2001)]; A.M. Pukhov, Phys. Rev. Lett. **86**, 3562 (2001); Y. Sentoku *et al.*, Appl. Phys. B: Lasers Opt. **B74**, 207 (2002); T. Nakamura, Phys. Rev. E **67**, 026403 (2003); S. Bulanov *et al.*, Plasma Phys. Rep. **28**, 975 (2002).

[8] R.A. Kishek *et al.*, Phys. Plasmas **10**, 2016 (2003).

[9] A.W. Chao *et al.*, Phys. Rev. ST Accel. Beams **6**, 024201 (2003).

[10] P. Chen *et al.*, IEEE Trans. Plasma Sci. **PS-15**, 218 (1987); J.J. Su *et al.*, Phys. Rev. A **41**, 3321 (1990).

[11] A. Mangeney *et al.*, J. Comput. Phys. **179**, 495 (2002).

[12] V.G. Ledenev *et al.*, Plasma Phys. Rep. **29**, 300 (2003).

[13] Y. Nishida *et al.*, Phys. Rev. Lett. **66**, 2328 (1991).
[14] O. Buneman, Phys. Rev. Lett. **1**, 8 (1958).
[15] S.V. Bulanov *et al.*, Zh. Eksp. Teor. Fiz. **72**, 1809 (1977) [Sov. Phys. JETP **45**, 949 (1977)].
[16] S. Bulanov *et al.*, Phys. Rev. E **58**, R5257 (1998).
[17] J. M. Dawson *et al.*, in *Proceedings of the Third InternationalConference on Plasma Physics and Controlled Nuclear Fusion Research, Novosibirsk 1968* (IAEA, Vienna, 1969), p. 735.
[18] B. Li *et al.*, Phys. Plasmas **9**, 2976 (2002); T. Umeda, *ibid* **10**, 382 (2003).
[19] A.B. Mikhailovskii, *Theory of Plasma Instabilities* (Consultants Bureau, New York, 1974), Vol. 1, p. 87.
[20] N. A. Krall and A. T. Trivelpiece, *Principles of Plasma Physics* (San Francisco Press, San Francisco, 1986).
[21] V.E. Zakharov, Zh. Eksp. Teor. Fiz. **62**, 1745 (1972) [Sov. Phys. JETP **35**, 908 (1972)]; F. Califano and M. Lontano, Phys. Rev. Lett. **83**, 96 (1999); A.S. Kingsep *et al.*, *ibid.* **31**, 1482 (1973); M.V. Goldman *et al.*, *ibid.* **70**, 4075 (1993).